

# Nonlinear Buckling Analysis of Piezothermoelastic Composite Plates

Balasubramanian Datchanamourty<sup>a</sup> and George E. Blandford<sup>a1</sup>

<sup>a</sup>Ph.D. Graduate and Professor  
Department of Civil Engineering, University of Kentucky, Lexington, KY 40506, USA

## Abstract

A geometric nonlinear finite element formulation for deformable piezothermoelastic composite laminates using first-order shear deformation theory is presented to solve mechanically and self-strained (thermal and electric field) loaded smart composite plate buckling problems. Green-Lagrange strain-displacement equations in the von Karman sense represent geometric nonlinearity. Mixed finite elements using hierarchic Lagrangian interpolation functions are used for the inplane and transverse displacements and electric potential variations, whereas transverse shear stress resultants at the Gauss quadrature points use standard Lagrangian shape functions. Geometrically nonlinear and eigenvalue (bifurcation) analyses are used to determine the critical buckling load magnitudes and corresponding mode shapes. The investigation on the buckling behavior of smart composite plates includes the direct piezoelectric effect on the buckling load magnitudes.

**KEYWORDS:** buckling, direct piezoelectric effect, geometric nonlinearity, and smart composite

---

<sup>1</sup> Corresponding author: Telephone number – (859) 257-1855; Fax number – (859) 257-4404; and e-mail – [gebland@engr.uky.edu](mailto:gebland@engr.uky.edu)

# 1. Background

Piezoelectric materials exhibit the property of generating an electric potential when subjected to mechanical deformations and this phenomenon is the direct piezoelectric effect. The converse piezoelectric effect by which the material changes shape when an electric voltage is applied is widely used in the actuation and control of vibration in mechanical devices. Piezoelectric materials, also known as smart materials, find their application in aerospace structures, piezoelectric motors, ultrasonic transducers, microphones, etc. Configuring smart composite structures involves bonding piezoelectric layers to the top and bottom of a multilayered composite elastic laminate. The piezoelectric layers act as distributed sensor and actuator to monitor and control the static and dynamic response of the structure.

Extensive studies on plate buckling under mechanical loads are available in the literature starting from the late 50's, e.g., Timoshenko and Gere (1961). Thermal buckling of composite laminates gained importance only within the last two decades and a very limited number of reports are available in the area of piezothermoelastic buckling. The effect of coupled piezoelectricity on the critical buckling load of laminated plates due to mechanical and thermal loads is a topic of recent research.

Gossard et al. (1952) are one of the earliest to investigate buckling problems under thermal loading. They predicted the buckling response of isotropic plates utilizing the Rayleigh-Ritz method. Tauchert (1987) analyzed the buckling behavior of moderately thick simply supported anti-symmetric angle-ply laminates subjected to a uniform temperature rise. He employed the thermoelastic version of Reissner-Mindlin plate theory to represent the transverse shear deformation. Tauchert and Huang (1987) and Huang and Tauchert

(1992) studied the buckling of symmetric angle-ply laminated plates using classical plate theory and first-order shear deformation theory, respectively. Chen and Chen (1989) employed a finite element approach to study the thermal buckling behavior of laminated plates subjected to a nonuniform temperature distribution. They used products of one-dimensional, cubic Hermitian polynomials to approximate the displacement variables at the midsurface of the plate. Noor and Peters (1992) investigated the thermomechanical buckling behavior of composite plates under the action of combined thermal and axial loads based on the first-order shear deformation theory. They employed a mixed finite element formulation with the generalized displacements and plate stress resultants as unknown variables. Other investigators who studied thermal buckling of composite laminates include Prabhu and Dhanaraj (1994), Chandrashekhara (1990), Thangaratnam and Ramachandran (1989), and Chen et al. (1991).

Jonnalagadda (1993) reported a third-order displacement theory to analyze bending and buckling of piezothermoelastic composite plates. He considered only the converse piezoelectric effect and does not include piezoelectric coupling. He investigated bending and buckling of composite laminates under thermal and electric loading and compared the results of various higher order theories. Dawe and Ge (2000) developed a spline finite strip method for predicting the critical buckling temperatures of rectangular composite laminated plates with various boundary conditions. They used FSDT and assumed a nonuniform temperature distribution in the plane of the plate. Shukla and Nath (2002) developed an analytical formulation to study the postbuckling response of moderately thick composite laminates under the action of inplane mechanical and thermal loadings using a Chebyshev series method.

Varelis and Saravanos (2002) formulated a geometric nonlinear, coupled formulation for composite piezoelectric plate structures using eight node two-dimensional finite elements. They predicted buckling of multilayered beams and plates and studied the effects of electromechanical coupling on the buckling load. In a later paper, Varelis and Saravanos (2004) presented a coupled mixed-field laminate theory to predict the pre and postbuckling response of composite laminates with piezoelectric actuators and sensors. They also analyzed piezoelectric buckling and postbuckling induced by actuators. Tzou and Zhou (1997) developed a theoretical formulation to investigate the dynamics, electromechanical coupling effects, and control of thermal buckling of piezoelectric laminated circular plates with an initial large deformation. They also studied the active control of nonlinear deflections, thermal buckling, and natural frequencies of the plate using high control voltages. Kabir et al. (2007) presented an analytical approach for the thermal buckling response of moderately thick symmetric angle-ply laminates with clamped boundary conditions based on first-order shear deformation theory.

In this paper, a mixed finite element formulation for piezothermoelastic composite laminates based on Reissner-Mindlin plate theory is used. Geometric nonlinearity in the von Karman sense is considered. Displacement and electric potential degrees of freedom are discretized using hierarchic quadratic, cubic, and quartic Lagrangian finite elements (e.g., Zienkiewicz and Taylor 2000). Element level transverse shear stress resultants, interpolated at the Gauss quadrature points using standard Lagrangian shape functions, are condensed. Nodal temperatures vary linearly through the entire depth of the plate while electric potentials change piecewise linearly through the laminate thickness. Eigenvalue and

geometrically nonlinear analysis results for both mechanical and self-strained loadings are investigated. These results demonstrate the piezoelectric coupling effect on the critical loads.

## 2. Governing Equations

Constitutive equations for a typical layer  $k$  of a multilayered piezothermoelastic composite laminate in the Reissner-Mindlin sense relative to the plate geometric coordinate axes  $x$ ,  $y$  and  $z$  are (see Figure 1 and Appendix A of Jonnalagadda et al. 1994))

$$\{\sigma\}_k = [\bar{Q}]_k \{\varepsilon\}_k - [\bar{e}]_k^T \{E\}_k - \{\bar{\lambda}\}_k \tilde{\theta} \quad (1a)$$

$$\begin{Bmatrix} \sigma_x \\ \sigma_y \\ \tau_{xy} \\ \tau_{yz} \\ \tau_{xz} \end{Bmatrix}_k = \begin{bmatrix} \bar{Q}_{11} & \bar{Q}_{12} & \bar{Q}_{16} & 0 & 0 \\ \bar{Q}_{12} & \bar{Q}_{22} & \bar{Q}_{26} & 0 & 0 \\ \bar{Q}_{16} & \bar{Q}_{26} & \bar{Q}_{66} & 0 & 0 \\ \hline 0 & 0 & 0 & \bar{Q}_{44} & \bar{Q}_{45} \\ 0 & 0 & 0 & \bar{Q}_{45} & \bar{Q}_{55} \end{bmatrix}_k \begin{Bmatrix} \varepsilon_x \\ \varepsilon_y \\ \gamma_{xy} \\ \gamma_{yz} \\ \gamma_{xz} \end{Bmatrix} - \begin{bmatrix} 0 & 0 & 0 & \bar{e}_{14} & \bar{e}_{15} \\ 0 & 0 & 0 & \bar{e}_{24} & \bar{e}_{25} \\ \hline \bar{e}_{31} & \bar{e}_{32} & \bar{e}_{36} & 0 & 0 \end{bmatrix}_k^T \begin{Bmatrix} E_x \\ E_y \\ E_z \end{Bmatrix}_k - \begin{Bmatrix} \bar{\lambda}_x \\ \bar{\lambda}_y \\ \bar{\lambda}_{xy} \\ 0 \\ 0 \end{Bmatrix}_k \tilde{\theta} \quad (1b)$$

$$\{D\}_k = [\bar{e}]_k \{\varepsilon\}_k + [\bar{\eta}]_k \{E\}_k + \{\bar{P}_\theta\}_k \tilde{\theta} \quad (2a)$$

$$\begin{Bmatrix} D_x \\ D_y \\ D_z \end{Bmatrix}_k = \begin{bmatrix} 0 & 0 & 0 & \bar{e}_{14} & \bar{e}_{15} \\ 0 & 0 & 0 & \bar{e}_{24} & \bar{e}_{25} \\ \hline \bar{e}_{31} & \bar{e}_{32} & \bar{e}_{36} & 0 & 0 \end{bmatrix}_k \begin{Bmatrix} \varepsilon_x \\ \varepsilon_y \\ \gamma_{xy} \\ \gamma_{yz} \\ \gamma_{xz} \end{Bmatrix} + \begin{bmatrix} \bar{\eta}_{11} & \bar{\eta}_{12} & 0 \\ \bar{\eta}_{12} & \bar{\eta}_{22} & 0 \\ \hline 0 & 0 & \bar{\eta}_{33} \end{bmatrix}_k \begin{Bmatrix} E_x \\ E_y \\ E_z \end{Bmatrix}_k + \begin{Bmatrix} 0 \\ 0 \\ \bar{P}_z \end{Bmatrix}_k \tilde{\theta} \quad (2b)$$

where  $\{\sigma\}$  = second Piola-Kirchhoff stress vector which is the work conjugate of Green-Lagrange strain vector  $\{\varepsilon\}$ ;  $\{E\}$  = electric field vector;  $\{\bar{\lambda}\}$  = temperature-stress vector;  $\tilde{\theta} = \theta - \theta_R$ ;  $\theta$  = temperature;  $\theta_R$  = reference temperature;  $\{D\}$  = electric displacement vector;  $\{\bar{P}_\theta\}$  = pyroelectric vector;  $[\bar{Q}]$  = material stiffness matrix;  $[\bar{e}]$  = piezoelectric material matrix; and  $[\bar{\eta}]$  = electric permittivity matrix. The over bar in the material coefficient matrices and vectors denote transformation from the principal material axes to the laminate Cartesian coordinate system. For non-piezoelectric lamina, the piezoelectric terms are zero.

The plate displacements are

$$\begin{aligned} u(x, y, z) &= u^0(x, y) - z\phi_x(x, y) \\ v(x, y, z) &= v^0(x, y) - z\phi_y(x, y) \\ w(x, y, z) &= w^0(x, y) \end{aligned} \quad (3)$$

where  $u$ ,  $v$ , and  $w$  are the inplane displacements along the  $x$ ,  $y$  and  $z$  axes, respectively; superscript  $^0$  denotes midplane displacement; and  $\phi_x$  and  $\phi_y$  are rotations about the negative  $y$ -axis and positive  $x$ -axis, respectively.

The Green-Lagrange strain vector components in terms of the displacements with the nonlinear strains included in the von Karman sense (e.g., Reddy 2004) are

$$\begin{Bmatrix} \varepsilon_x \\ \varepsilon_y \\ \gamma_{xy} \end{Bmatrix} = \begin{Bmatrix} \varepsilon_x^0 \\ \varepsilon_y^0 \\ \gamma_{xy}^0 \end{Bmatrix} + z \begin{Bmatrix} \kappa_x \\ \kappa_y \\ \kappa_{xy} \end{Bmatrix} + \begin{Bmatrix} \varepsilon_x^N \\ \varepsilon_y^N \\ \gamma_{xy}^N \end{Bmatrix}$$

$$\begin{aligned}
&= \begin{bmatrix} \frac{\partial}{\partial x} & 0 \\ 0 & \frac{\partial}{\partial y} \\ \frac{\partial}{\partial y} & \frac{\partial}{\partial x} \end{bmatrix} \begin{Bmatrix} u^0 \\ v^0 \end{Bmatrix} + z \begin{bmatrix} -\frac{\partial}{\partial x} & 0 \\ 0 & -\frac{\partial}{\partial y} \\ -\frac{\partial}{\partial y} & -\frac{\partial}{\partial x} \end{bmatrix} \begin{Bmatrix} \phi_x \\ \phi_y \end{Bmatrix} + \frac{1}{2} \begin{bmatrix} \frac{\partial w^0}{\partial x} & 0 \\ 0 & \frac{\partial w^0}{\partial y} \\ \frac{\partial w^0}{\partial y} & \frac{\partial w^0}{\partial x} \end{bmatrix} \begin{Bmatrix} \frac{\partial}{\partial x} \\ \frac{\partial}{\partial y} \end{Bmatrix} w^0 \\
&= [D_\varepsilon] \begin{Bmatrix} u^0 \\ v^0 \end{Bmatrix} + [D_\kappa] \begin{Bmatrix} \phi_x \\ \phi_y \end{Bmatrix} + \frac{1}{2} [A_\phi(w)] \{D_N\} w^0 = \{\varepsilon^0\} + z \{\kappa\} + \{\varepsilon_N\} \quad (4a)
\end{aligned}$$

$$\begin{Bmatrix} \gamma_{yz} \\ \gamma_{xz} \end{Bmatrix} = \begin{bmatrix} \frac{\partial}{\partial y} & 0 & -1 \\ \frac{\partial}{\partial x} & -1 & 0 \end{bmatrix} \begin{Bmatrix} w^0 \\ \phi_x \\ \phi_y \end{Bmatrix} = \begin{bmatrix} \{^w D\} & -[I_s] \end{bmatrix} \begin{Bmatrix} w^0 \\ \phi_x \\ \phi_y \end{Bmatrix} = \{\varepsilon_s\} \quad (4b)$$

The strain expressions in equations (4a) – (4b) can be expressed more compactly as

$$\{\varepsilon_b\} = \{\varepsilon_b^L\} + \{\varepsilon^N\} = \left[ [D_b^L] + \frac{1}{2} [D^N(w)] \right] \{\hat{u}\} \quad (5a)$$

$$\{\varepsilon_s\} = [D_s] \{\hat{u}\} \quad (5b)$$

$$\text{where } [D_b^L] = \begin{bmatrix} [D_\varepsilon] & \{0\}_{3 \times 1} & [0]_{3 \times 2} \\ [0]_{3 \times 2} & \{0\}_{3 \times 1} & [D_\kappa] \end{bmatrix}; \quad [D^N(w)] = \begin{bmatrix} [0]_{3 \times 2} & [A_\phi(w)] \{D_N\} & [0]_{3 \times 2} \\ [0]_{3 \times 2} & \{0\}_{3 \times 1} & [0]_{3 \times 2} \end{bmatrix};$$

$$[D_s] = \begin{bmatrix} [0]_{2 \times 2} & \{^w D\} & -[I_s] \end{bmatrix}; \quad \{\varepsilon_b^L\} = \langle\langle \varepsilon^0 \rangle \rangle \langle \kappa \rangle \rangle^T = \text{linear strain vector};$$

$$\{\varepsilon^N\} = \langle\langle \varepsilon_N \rangle \rangle \langle 0 \rangle \rangle^T = \text{nonlinear strain vector}; \quad \text{and } \{\hat{u}\} = \langle u^0 \ v^0 \ w^0 \ \phi_x \ \phi_y \rangle^T.$$

The electric field vector, which is the negative of the potential gradient, is

$$\langle E_x \ E_y \ E_z \rangle^T = - \left\langle \frac{\partial \psi}{\partial x} \ \frac{\partial \psi}{\partial y} \ \frac{\partial \psi}{\partial z} \right\rangle^T = - \{\nabla\} \psi(x, y, z) \quad (6)$$

where  $\{\nabla\} = \langle \partial / \partial x \ \partial / \partial y \ \partial / \partial z \rangle^T$  = gradient vector. Electric potential  $\psi$  is assumed to

vary piecewise linearly through the thickness of a piezoelectric layer  $\rho$

$$\begin{aligned}\psi^\rho(x, y, z) &= \left( \frac{z_{\rho+1} - z}{t_\rho} \right) \psi_b^\rho(x, y) + \left( \frac{z - z_\rho}{t_\rho} \right) \psi_t^\rho(x, y) \\ &= \left\langle M_{\psi 1}^\rho(z) \quad M_{\psi 2}^\rho(z) \right\rangle \begin{Bmatrix} \psi_b^\rho(x, y) \\ \psi_t^\rho(x, y) \end{Bmatrix} = \left\langle M_\psi^\rho(z) \right\rangle \{\psi^\rho(x, y)\}\end{aligned}\quad (7)$$

where subscripts t, b = top, bottom of the piezoelectric layer;  $\psi_b^\rho$ ,  $\psi_t^\rho$  = electric potential at the bottom and top of the piezoelectric layer  $\rho$ ; and  $t_\rho$  = thickness of piezoelectric layer  $\rho$ .

Substituting equation (7) into equation (6) gives

$$\{E\}_\rho = -\{\nabla\} \left\langle M_\psi^\rho(z) \right\rangle \{\psi^\rho(x, y)\} = -[Z_\psi^\rho][D_\psi^\rho]\{\psi^\rho(x, y)\}\quad (8)$$

where

$$[Z_\psi^\rho] = \begin{bmatrix} M_{\psi 1} & M_{\psi 2} & 0 & 0 & 0 & 0 \\ 0 & 0 & M_{\psi 1} & M_{\psi 2} & 0 & 0 \\ 0 & 0 & 0 & 0 & -1/t_\rho & 1/t_\rho \end{bmatrix} \begin{array}{l} \text{electric potential} \\ \text{depth interpolation} \\ \text{matrix; and} \end{array}\quad (9a)$$

$$[D_\psi^\rho] = \begin{bmatrix} \frac{\partial}{\partial x} & 0 & \frac{\partial}{\partial y} & 0 & 1 & 0 \\ 0 & \frac{\partial}{\partial x} & 0 & \frac{\partial}{\partial y} & 0 & 1 \end{bmatrix}^T = \begin{array}{l} \text{electric potential inplane} \\ \text{gradient matrix.} \end{array}\quad (9b)$$

Applying thermal loading by specifying the temperature on the top and bottom surfaces of the laminate induces thermoelastic and pyroelectric effects. Assuming  $\tilde{\theta}$  varies linearly through the entire depth of the plate

$$\begin{aligned}\tilde{\theta}(x, y, z) &= \left( \frac{1}{2} - \frac{z}{h} \right) \tilde{\theta}_b(x, y) + \left( \frac{1}{2} + \frac{z}{h} \right) \tilde{\theta}_t(x, y) \\ &= \left\langle M_{\theta 1}(z) \quad M_{\theta 2}(z) \right\rangle \begin{Bmatrix} \tilde{\theta}_b(x, y) \\ \tilde{\theta}_t(x, y) \end{Bmatrix} = \left\langle M_\theta(z) \right\rangle \{\tilde{\theta}(x, y)\}\end{aligned}\quad (10)$$

where  $\tilde{\theta}_b, \tilde{\theta}_t$  = bottom and top surface temperatures of the plate at  $z = -h/2$  and  $z = h/2$ , respectively. Using equations (7) and (10), the stress and electric displacement equations in terms of inplane and transverse components are

$$\begin{aligned} \begin{Bmatrix} \{\sigma_p\} \\ \{\sigma_s\} \end{Bmatrix}_k &= \begin{bmatrix} [\bar{Q}_p] & [0] \\ [0] & [\bar{Q}_s] \end{bmatrix}_k \begin{Bmatrix} \{\varepsilon_p\} \\ \{\varepsilon_s\} \end{Bmatrix}_k + \begin{bmatrix} [0] & [\bar{e}_s] \\ \langle \bar{e}_p \rangle & \langle 0 \rangle \end{bmatrix}_k^T [Z_\psi^p][D_\psi^p]\{\psi^p(x, y)\} \\ &- \begin{Bmatrix} \{\bar{\lambda}_p\} \\ \{0\} \end{Bmatrix}_k \langle M_\theta(z) \rangle \{\hat{\theta}(x, y)\} \end{aligned} \quad (11a)$$

$$\begin{aligned} \begin{Bmatrix} \{D_s\} \\ D_p \end{Bmatrix}_\rho &= \begin{bmatrix} [0] & [\bar{e}_s] \\ \langle \bar{e}_p \rangle & \langle 0 \rangle \end{bmatrix}_\rho \begin{Bmatrix} \{\varepsilon_p\} \\ \{\varepsilon_s\} \end{Bmatrix}_\rho - \begin{bmatrix} [\bar{\eta}_s] & \{0\} \\ \langle 0 \rangle & \bar{\eta}_p \end{bmatrix}_\rho [Z_\psi^p][D_\psi^p]\{\psi^p(x, y)\} \\ &+ \begin{Bmatrix} \{0\} \\ \bar{P}_{p\theta} \end{Bmatrix}_\rho \langle M_\theta(z) \rangle \{\hat{\theta}(x, y)\} \end{aligned} \quad (11b)$$

where p, s = inplane, transverse shear components; and  $\bar{P}_{p\theta} = \bar{P}_z$ .

The stress resultants per unit width of the plate are

$$\{\{N\}, \{M\}, \{Q\}\} = \int_{-h/2}^{+h/2} (\{\sigma_p\}, z\{\sigma_p\}, \{\sigma_s\}) dz \quad (12)$$

where  $h$  = plate thickness;  $\{N\} = \langle N_x \quad N_y \quad N_{xy} \rangle^T$  = inplane stress resultant vector;  $\{M\} = \langle M_x \quad M_y \quad M_{xy} \rangle^T$  = moment resultant vector; and  $\{Q\} = \langle Q_y \quad Q_x \rangle^T$  = transverse shear stress resultant vector. The resulting constitutive equations are

$$\begin{Bmatrix} \{N\} \\ \{M\} \end{Bmatrix} = \begin{bmatrix} [A] & [B] \\ [B] & [D] \end{bmatrix} \begin{Bmatrix} \{\varepsilon^o\} + \{\varepsilon_N\} \\ \{\kappa\} \end{Bmatrix} + \begin{bmatrix} [A_e]^T \\ [B_e]^T \end{bmatrix} \{\hat{\psi}\} - \begin{bmatrix} [A_\lambda] \\ [B_\lambda] \end{bmatrix} \{\hat{\theta}\} \quad (13a)$$

$$\{Q\} = [S]\{\varepsilon_s\} + [S_e^1]^T \frac{\partial}{\partial x} \{\hat{\psi}\} + [S_e^2]^T \frac{\partial}{\partial y} \{\hat{\psi}\} \quad (13b)$$

Using the strain-displacement equations (4a, b) and (5a, b), the stress resultants are

$$\begin{aligned} \{\bar{N}\} &= [C]([D_b^L] + \frac{1}{2}[D^N(w)])\{\hat{u}\} + [C_e]^T \{\hat{\psi}\} - [\Lambda]\{\hat{\theta}\} \\ &= \langle \langle N \rangle \quad \langle M \rangle \rangle^T = \{\bar{N}^u\} + \{\bar{N}^\psi\} - \{\bar{N}^\theta\} \end{aligned} \quad (14a)$$

$$\{Q\} = [S][D_s]\{\hat{u}\} + [S_e]^T [D_\psi]\{\hat{\psi}\} = \{Q^u\} + \{Q^\psi\} \quad (14b)$$

where  $\{\bar{N}^\alpha\} = \langle \langle N^\alpha \rangle \quad \langle M^\alpha \rangle \rangle^T$ ;  $\{N^\alpha\} = \langle N_x^\alpha \quad N_y^\alpha \quad N_{xy}^\alpha \rangle^T$ ;  $\{M^\alpha\} =$

$\langle M_x^\alpha \quad M_y^\alpha \quad M_{xy}^\alpha \rangle^T$ ;  $\{Q^\alpha\} = \langle Q_y^\alpha \quad Q_x^\alpha \rangle^T$ ; and  $\alpha = u, \psi$  or  $\theta$ . The electric potential

inplane gradient matrix and electric potential vector for the laminate are

$$[D_\psi] = \text{diag} \left[ [D_\psi^1] \quad [D_\psi^2] \quad \dots \quad [D_\psi^{NP}] \right] \quad (15a)$$

$$\{\hat{\psi}\} = \left\langle \langle \psi_b^1 \quad \psi_t^1 \rangle \quad \langle \psi_b^2 \quad \psi_t^2 \rangle \quad \dots \quad \langle \psi_b^{NP} \quad \psi_t^{NP} \rangle \right\rangle^T \quad (15b)$$

Depth integrated material coefficient matrices for the laminate are

$$[C] = \begin{bmatrix} [A] & [B] \\ [B] & [D] \end{bmatrix}; [C_e]^T = \begin{bmatrix} [A_e]^T \\ [B_e]^T \end{bmatrix}; [\Lambda] = \begin{bmatrix} [A_\lambda] & [B_\lambda] \end{bmatrix}^T \quad (16a, b, c)$$

$$([A], [B], [D]) = \sum_{k=1}^{NL} [\bar{Q}_p]_k \left( (z_{k+1} - z_k), \frac{1}{2}(z_{k+1}^2 - z_k^2), \frac{1}{3}(z_{k+1}^3 - z_k^3) \right) \quad (16d)$$

$$[A_e]^T = \left[ [A_e]_1^T \quad [A_e]_2^T \quad \dots \quad [A_e]_{NP}^T \right] \quad (16e)$$

$$[B_e]^T = \left[ [B_e]_1^T \quad [B_e]_2^T \quad \dots \quad [B_e]_{NP}^T \right] \quad (16f)$$

$$[A_e]_\rho = \begin{Bmatrix} -1 \\ 1 \end{Bmatrix} \langle \bar{e}_\rho \rangle_\rho; [B_e]_\rho = \frac{1}{2}(z_{\rho+1} + z_\rho)[A_e]_\rho \quad (16g, h)$$

$$[A_\lambda] = \left[ \frac{1}{2}\{\bar{A}_\lambda\} - \frac{1}{h}\{\bar{B}_\lambda\} \quad \frac{1}{2}\{\bar{A}_\lambda\} + \frac{1}{h}\{\bar{B}_\lambda\} \right] \quad (16i)$$

$$[\mathbf{B}_\lambda] = \left[ \frac{1}{2} \{\bar{\mathbf{B}}_\lambda\} - \frac{1}{h} \{\bar{\mathbf{D}}_\lambda\} \quad \frac{1}{2} \{\bar{\mathbf{B}}_\lambda\} + \frac{1}{h} \{\bar{\mathbf{D}}_\lambda\} \right] \quad (16j)$$

$$(\{\bar{\mathbf{A}}_\lambda\}, \{\bar{\mathbf{B}}_\lambda\}, \{\bar{\mathbf{D}}_\lambda\}) = \sum_{k=1}^{NL} \{\bar{\lambda}_p\}_k \left( (z_{k+1} - z_k), \frac{1}{2}(z_{k+1}^2 - z_k^2), \frac{1}{3}(z_{k+1}^3 - z_k^3) \right) \quad (16k)$$

$$[\mathbf{S}] = [\mathbf{K}_s] \sum_{k=1}^{NL} [\bar{\mathbf{Q}}_s]_k (z_{k+1} - z_k) [\mathbf{K}_s] \quad (16l)$$

$$[\mathbf{S}_e]^T = \left[ [\mathbf{S}_e]_1^T \quad [\mathbf{S}_e]_2^T \quad \cdots \quad [\mathbf{S}_e]_{NP}^T \right]; [\mathbf{S}_e]_\rho^T = \left[ [\mathbf{S}_e^1]_\rho^T \quad [\mathbf{S}_e^2]_\rho^T \quad [0] \right] \quad (16m, n)$$

$$[\mathbf{S}_e^1]_\rho = \frac{t_\rho}{2} \begin{bmatrix} \bar{e}_{14} & \bar{e}_{15} \\ \bar{e}_{14} & \bar{e}_{15} \end{bmatrix}; [\mathbf{S}_e^2]_k = \frac{t_\rho}{2} \begin{bmatrix} \bar{e}_{24} & \bar{e}_{25} \\ \bar{e}_{24} & \bar{e}_{25} \end{bmatrix}_\rho \quad (16o, p)$$

where NP = number of piezoelectric layers; and NL = total number of layers. Since the actual variation of transverse shear stresses in a plate is not constant through the depth,

Reissner-Mindlin theory introduces a shear correction matrix  $[\mathbf{K}_s] = \begin{bmatrix} k_{s2} & 0 \\ 0 & k_{s1} \end{bmatrix}$  in the

depth integrated transverse shear coefficient matrix. Coefficients  $k_{s1}$  and  $k_{s2}$  are shear

correction factors. Electric potential between adjacent layers is continuous. This paper

assumes that a grounded interface exists between a piezoelectric layer and a structural layer,

i.e., electric potential is zero.

### 3. Coupled Mixed Variational Principle

Using the modified Hellinger-Reissner functional facilitates independent interpolation of displacement, electric potential and transverse shear stress resultant variables. The depth integrated mechanical energy functional for a mixed variational formulation is

$$\Pi^M = \frac{1}{2} \int_A \left\{ ([D_b^L] + \frac{1}{2}[D^N(w)]) \{\bar{\mathbf{u}}\} \right\}^T [\mathbf{C}] \left\{ ([D_b^L] + \frac{1}{2}[D^N(w)]) \{\bar{\mathbf{u}}\} \right\} dA$$

$$\begin{aligned}
& + \int_A \{[D_s]\{\hat{u}\}\}^T \{Q\} dA - \frac{1}{2} \int_A \langle Q \rangle [S]^{-1} \{Q\} dA \\
& - \int_A \left\{ [D_b^L] + \frac{1}{2} [D^N(w)] \{\hat{u}\} \right\}^T [\Lambda] \{\hat{\theta}\} dA \\
& + \frac{1}{2} \int_A \left\{ [D_b^L] + \frac{1}{2} [D^N(w)] \{\hat{u}\} \right\}^T [C_e]^T \{\hat{\psi}\} dA \\
& + \int_A \langle Q \rangle [S]^{-1} \left( [S_e]^T [D_\psi] \{\hat{\psi}\} \right) dA - \Pi_{\text{ext}}^M \tag{17}
\end{aligned}$$

where  $\Pi^M$  = modified Hellinger-Reissner functional that represents mechanical (elastic) energy;  $\Pi_{\text{ext}}^M$  = potential energy due to externally applied mechanical loads;  $A$  = plate area; and the other symbols are as previously defined.

The depth integrated piezoelectric energy functional is

$$\begin{aligned}
\Pi^P &= \frac{1}{2} \int_A \langle \hat{\psi} \rangle [C_e] \{\varepsilon_b\} dA + \frac{1}{2} \int_A \{[D_\psi] \{\hat{\psi}\}\}^T [S_e] \{\varepsilon_s\} dA \\
& - \frac{1}{2} \int_A \{[D_\psi] \{\hat{\psi}\}\}^T [C_\eta] [D_\psi] \{\hat{\psi}\} dA + \int_A \{[D_\psi] \{\hat{\psi}\}\}^T [P_\theta] \{\hat{\theta}\} dA - \Pi_{\text{ext}}^P \tag{18}
\end{aligned}$$

where  $\Pi^P$  = piezoelectric energy functional;  $\Pi_{\text{ext}}^P$  = external work due to applied electric potential; and the depth integrated dielectric and pyroelectric matrices for the laminate are

$$[C_\eta] = \text{diag} \left[ [C_\eta]_1 \ [C_\eta]_2 \ \cdots \ [C_\eta]_{NP} \right] \tag{19a}$$

$$[C_\eta]_\rho = \int_{z_\rho}^{z_{\rho+1}} [Z_\psi^\rho]^T [\bar{\eta}]_\rho [Z_\psi^\rho] dz = \begin{bmatrix} [\eta_{11}] & [\eta_{12}] & [0] \\ [\eta_{21}] & [\eta_{22}] & [0] \\ [0] & [0] & [\eta_{33}] \end{bmatrix}_\rho \tag{19b}$$

$$[\eta_{ij}]_\rho = \frac{(\bar{\eta}_{ij})_\rho t_\rho}{6} \begin{bmatrix} 2 & 1 \\ 1 & 2 \end{bmatrix} \quad (i, j = 1, 2); \quad [\eta_{33}]_\rho = \frac{(\bar{\eta}_{33})_\rho}{t_\rho} \begin{bmatrix} 1 & -1 \\ -1 & 1 \end{bmatrix} \tag{19c, d}$$

$$[P_\theta] = \text{diag} \left[ [P_\theta]_1 \ [P_\theta]_2 \ \cdots \ [P_\theta]_{NP} \right] \tag{19e}$$

$$[\mathbf{P}_\theta]_\rho = \int_{z_\rho}^{z_{\rho+1}} [\mathbf{Z}_\psi^\rho]^\top \begin{Bmatrix} 0 \\ 0 \\ \bar{\mathbf{P}}_z \end{Bmatrix}_\rho \langle M_\theta \rangle_\rho dz = \begin{bmatrix} [0]_{2 \times 2} \\ [0]_{2 \times 2} \\ [\bar{\mathbf{P}}]_\rho \end{bmatrix} \quad (19f)$$

$$[\bar{\mathbf{P}}]_\rho = -\frac{(\bar{\mathbf{P}}_z)_\rho}{2} \begin{bmatrix} 1 - \frac{z_{\rho+1} + z_\rho}{h} & 1 + \frac{z_{\rho+1} + z_\rho}{h} \\ -1 + \frac{z_{\rho+1} + z_\rho}{h} & -1 - \frac{z_{\rho+1} + z_\rho}{h} \end{bmatrix} \quad (19g)$$

## 4. Finite Element Approximation

The displacements, electric potentials, and transverse shear stress resultants in equations (17) and (18) are functions of the plate inplane coordinates. Thus, discretization uses two-dimensional finite elements. Hierarchic Lagrangian shape functions interpolate displacement and electric potential variables from Zienkiewicz and Taylor (2000) (see Fig. 2) are used to discretize the element displacement and electromagnetic potential variables. Interpolation of the transverse shear stress resultants  $Q_y$  and  $Q_x$  at the Gauss integration points (see Fig. 3) uses standard Lagrangian shape functions.

Under thermal loading, top and bottom surface temperatures are specified at the corner node points. Thus, temperature interpolation is based on the first four shape functions of Fig. 2(b).

Using the element shape functions, the element strain-displacement and electric displacement-electric potential matrices are

$$[\mathbf{B}_b^L] = [\mathbf{D}_b^L][\mathbf{N}_u] = [[\mathbf{B}_{b1}^L] \quad [\mathbf{B}_{b1}^L] \quad \cdots \quad [\mathbf{B}_{bnen}^L]] \quad (20a)$$

$$[\mathbf{B}_{bi}^L] = \begin{bmatrix} [\mathbf{B}_{ei}] & \{0\}_{3 \times 1} & [0]_{3 \times 2} \\ [0]_{3 \times 2} & \{0\}_{3 \times 1} & [\mathbf{B}_{ki}] \end{bmatrix} \quad (20b)$$

$$[\mathbf{B}_{ei}] = [\mathbf{D}_\varepsilon][\mathbf{I}_{Ni}] ; \quad [\mathbf{B}_{ki}] = [\mathbf{D}_\varepsilon][\mathbf{I}_{Ni}] \quad (20c, d)$$

$$[B_{ki}] = [D_k][I_{Ni}]; \quad [I_{Ni}] = \begin{bmatrix} N_i & 0 \\ 0 & N_i \end{bmatrix} \quad (20e, f)$$

$$[B_s] = [D_s][N_u] = [[B_{s1}] \quad [B_{s2}] \quad \cdots \quad [B_{s_{nen}}]] \quad (20g)$$

$$[B_{si}] = \begin{bmatrix} [0]_{2 \times 2} & \{^w B_i\} & -N_i[I_s] \end{bmatrix}; \quad \{^w B_i\} = \{^w D\}N_i \quad (20h, i)$$

$$[B^N] = [D^N][N_u] = [[B_1^N] \quad [B_2^N] \quad \cdots \quad [B_{nen}^N]] \quad (20j)$$

$$[B_i^N(w)] = \begin{bmatrix} [A_\phi(w)] \\ [0]_{3 \times 2} \end{bmatrix} [G]_i \quad (20k)$$

$$[A_\phi(w)] = \begin{bmatrix} \frac{\partial \langle N \rangle}{\partial x} \{w\} & 0 \\ 0 & \frac{\partial \langle N \rangle}{\partial y} \{w\} \\ \frac{\partial \langle N \rangle}{\partial y} \{w\} & \frac{\partial \langle N \rangle}{\partial x} \{w\} \end{bmatrix}; \quad [G]_i = \begin{bmatrix} 0 & 0 & \frac{\partial N_i}{\partial x} & 0 & 0 \\ 0 & 0 & \frac{\partial N_i}{\partial y} & 0 & 0 \end{bmatrix} \quad (20l, m)$$

$$[B_\psi] = [D_\psi][N_\psi] = [[B_{\psi 1}] \quad [B_{\psi 2}] \quad [B_{\psi 3}] \quad \cdots \quad [B_{\psi_{nen}}]] \quad (20n)$$

$$[B_{\psi i}] = [D_\psi][\hat{N}_{\psi i}] \quad (20o)$$

Combining the mechanical and piezoelectric energy functionals of equations (17) and (18), using equations (20a) – (20o), the total energy functional is

$$\begin{aligned} \Pi^e = & \langle \hat{u}^e \rangle \left[ \frac{1}{2} \int_a \{ [B_b^L] + \frac{1}{2} [B^N(w)] \}^T [C] \{ [B_b^L] + \frac{1}{2} [B^N(w)] \} da \right] \{ \hat{u}^e \} \\ & + \langle \hat{u}^e \rangle \left[ \int_a [B_s]^T [N_Q] da \right] \{ \hat{Q} \} - \langle \hat{Q} \rangle \left[ \frac{1}{2} \int_a [N_Q][S]^{-1}[N_Q]^T da \right] \{ \hat{Q}^e \} \\ & - \langle \hat{u}^e \rangle \left[ \int_a \{ [B_b^L] + \frac{1}{2} [B^N(w)] \}^T [\Lambda][N_\theta] da \right] \{ \hat{\theta}^e \} \\ & + \langle \hat{u}^e \rangle \left[ \int_a \{ [B_b^L] + \frac{1}{2} [B^N(w)] \}^T [C_e]^T [N_\psi] da \right] \{ \hat{\psi}^e \} \end{aligned}$$

$$\begin{aligned}
& + \langle \hat{Q}^e \rangle \left[ \int_a [N_Q]^T [S]^{-1} [S_e]^T [B_\psi] da \right] \{\hat{\psi}^e\} \\
& - \langle \hat{\psi}^e \rangle \left[ \frac{1}{2} \int_a \left( [B_\psi]^T [S_e] [S]^{-1} [S_e]^T [B_\psi] + [B_\psi]^T [C_\eta] [B_\psi] \right) da \right] \{\hat{\psi}^e\} \\
& + \langle \hat{\psi}^e \rangle \left[ \int_a [B_\psi]^T [P_\theta] [N_\theta] da \right] \{\hat{\theta}^e\} - \Pi_{\text{ext}}^e
\end{aligned} \tag{21}$$

where  $\Pi^e$  = total energy functional of element e;  $\Pi_{\text{ext}}^e$  = total external work due to mechanical and electrical loading of element e; and  $a$  = area of a typical element.

The structure reaches the state of equilibrium when the energy functional is stationary. Thus solution to the problem can be obtained by seeking a set of values for the degrees of freedom that renders the energy functional a stationary which is attained by taking a variation of the energy functional and equating it to zero. Taking the variation of the energy functional leads to the following matrix equations

$$\begin{aligned}
& \left( \begin{array}{ccc} [K^{uu}] & [K^{u\psi}] & [K^{uQ}] \\ [K^{\psi u}] & [K^{\psi\psi}] & [K^{\psi Q}] \\ [K^{Qu}] & [K^{Q\psi}] & [K^{QQ}] \end{array} \right)_e + \left( \begin{array}{ccc} [K_N^{uu}] & [K_N^{u\psi}] & [0] \\ [K_N^{\psi u}] & [0] & [0] \\ [0] & [0] & [0] \end{array} \right)_e \left\{ \begin{array}{c} \{\hat{u}^e\} \\ \{\hat{\psi}^e\} \\ \{\hat{Q}^e\} \end{array} \right\} - \left\{ \begin{array}{c} \{f_N^{u\theta}\} \\ \{0\} \\ \{0\} \end{array} \right\}_e \\
& = \left\{ \begin{array}{c} \{f^u\} \\ \{f^\psi\} \\ \{0\} \end{array} \right\}_e + \left\{ \begin{array}{c} \{f^{u\theta}\} \\ \{f^{\psi\theta}\} \\ \{0\} \end{array} \right\}_e
\end{aligned} \tag{22}$$

where  $\{\hat{u}^e\}_i$  and  $\{\hat{\psi}^e\}_i = i^{\text{th}}$  node displacement and potential vectors of element e;  $\{\hat{Q}^e\}_i = i^{\text{th}}$  node transverse shear stress resultants vector of element e;  $\{f^u\}_e =$  mechanical load vector of element e; and  $\{f^\psi\}_e =$  electrical load vector of element e. The element coefficient matrices and thermal load vectors are

$$[K^{uu}]_e = \int_a [B_b^L]^T [C] [B_b^L] da \quad (23a)$$

$$[K^{uQ}]_e = [K^{Qu}]_e^T = \int_a [B_s]^T [N_Q] da \quad (23b)$$

$$[K^{QQ}]_e = -\int_a [N_Q] [S]^{-1} [N_Q]^T da \quad (23c)$$

$$[K^{u\psi}]_e = [K^{\psi u}]_e^T = \int_a [B_b^L]^T [C_e]^T [N_\psi] da \quad (23d)$$

$$[K^{Q\psi}]_e = [K^{\psi Q}]_e^T = \int_a [N_Q]^T [S]^{-1} ([S_e]^T [B_\psi]) da \quad (23e)$$

$$[K^{\psi\psi}]_e = -\int_a [B_\psi]^T [S_e] [S]^{-1} [S_e]^T [B_\psi] da - \int_a [B_\psi]^T [C_\eta] [B_\psi] da \quad (23f)$$

$$[K_N^{uu}]_e = \int_a \left( \begin{array}{l} \{ [B_b^L] [C] (\frac{1}{2} [B^N(w)]) + [B^N(w)]^T [C] [B_b^L] \\ + [B^N(w)]^T [C] (\frac{1}{2} [B^N(w)]) \} \end{array} \right) da \quad (23g)$$

$$[K_N^{u\psi}]_e = \int_a [B^N(w)]^T [C_e]^T [N_\psi] da \quad (23h)$$

$$[K_N^{\psi u}]_e = \int_a [N_\psi]^T [C_e] (\frac{1}{2} [B^N(w)]) da \quad (23i)$$

$$\{f^{u\theta}\}_e = \left[ \int_a [B_b^L] [\Lambda] [N_\theta] da \right] \{\hat{\theta}^e\} \quad (23j)$$

$$\{f_N^{u\theta}\}_e = \left[ \int_a [B^N(w)]^T [\Lambda] [N_\theta] da \right] \{\hat{\theta}^e\} \quad (23k)$$

$$\{f^{\psi\theta}\}_e = \left[ \int_a [B_\psi]^T [P_\theta] [N_\theta] da \right] \{\hat{\theta}^e\} \quad (23l)$$

where  $[N_\psi] = [\hat{N}_{\psi 1} \ \hat{N}_{\psi 2} \ \cdots \ \hat{N}_{\psi \text{nen}}]$ ;  $[\hat{N}_{\psi i}] =$

$$= \begin{bmatrix} N_i & 0 & \cdots & 0 \\ 0 & N_i & \cdots & 0 \\ 0 & N_i & \cdots & 0 \\ \vdots & \vdots & \ddots & \vdots \\ 0 & 0 & \cdots & N_i \end{bmatrix}_{2NP \times (NP+1)}$$

electric potential shape function matrix which enforces continuity of the variables between adjacent layers;  $[N_u] = [N_1[I_5] \ N_2[I_5] \ \cdots \ N_{\text{nen}}[I_5]]$ ;  $[N_\theta] = [N_1[I_2] \ N_2[I_2] \ N_3[I_2] \ N_4[I_2]]$ ;  $\hat{\theta}_j = j^{\text{th}}$  corner node temperature;  $N_i = i^{\text{th}}$  hierarchical shape function (see Fig. 2);  $[I_k] = k \times k$  identity matrix;  $\text{nen} =$  number of element nodes;  $[N_Q] = [\bar{N}_1[I_2] \ \bar{N}_2[I_2] \ \cdots \ \bar{N}_{\text{nens}}[I_2]]$ ;  $\bar{N}_i =$  Lagrangian shape function corresponding to the  $i^{\text{th}}$  transverse shear interpolation point (see Fig. 3); and  $\text{nens} =$  number of element transverse shear stress resultant interpolation points.

Condensation of the non-continuous element transverse shear stress resultants at the element level simplifies the element matrix equations of (22), which leads to

$$[\bar{K}_L]_e + [K_N]_e \{U^e\} - \{f_N\}_e = \{f^U\}_e + \{f^\theta\}_e \quad (24)$$

where

$$[\bar{K}_L]_e = [K^{UU}]_e - [K^{QU}]_e^T [K^{QQ}]_e^{-1} [K^{QU}]_e \quad (25a)$$

$$\left( \begin{array}{c|c} [K^{UU}] & [K^{UQ}] \\ \hline [K^{QU}] & [K^{QQ}] \end{array} \right)_e = \left( \begin{array}{c|c} [K^{uu}] & [K^{u\psi}] \\ \hline [K^{\psi u}] & [K^{\psi\psi}] \\ \hline [K^{Qu}] & [K^{Q\psi}] \\ \hline & [K^{QQ}] \end{array} \right)_e$$

$$[\bar{K}_L]_e = \left( \begin{array}{c|c} [\bar{K}^{uu}] & [\bar{K}^{u\psi}] \\ \hline [\bar{K}^{\psi u}] & [\bar{K}^{\psi\psi}] \end{array} \right)_e; \quad [K_N]_e = \left( \begin{array}{c|c} [K_N^{uu}] & [K_N^{u\psi}] \\ \hline [K_N^{\psi u}] & [0] \end{array} \right)_e \quad (25b, c)$$

$$\{\mathbf{U}^e\} = \begin{Bmatrix} \{\hat{\mathbf{u}}^e\} \\ \{\hat{\boldsymbol{\psi}}^e\} \end{Bmatrix}; \quad \{\mathbf{f}_N\}_e = \begin{Bmatrix} \{\mathbf{f}_N^{u\theta}\} \\ \{\mathbf{0}\} \end{Bmatrix}_e \quad (25d, e)$$

$$\{\mathbf{f}^U\}_e = \begin{Bmatrix} \{\mathbf{f}^u\} \\ \{\mathbf{f}^\psi\} \end{Bmatrix}_e; \quad \{\mathbf{f}^\theta\}_e = \begin{Bmatrix} \{\mathbf{f}^{u\theta}\} \\ \{\mathbf{f}^{\psi\theta}\} \end{Bmatrix}_e \quad (25f, g)$$

The over bar denotes condensed matrices.

Assembly of the element equilibrium equations (24) uses the direct stiffness method to obtain the structure equations. Global equilibrium equations are

$$[[\bar{\mathbf{K}}_L] + [\mathbf{K}_N]]\{\mathbf{U}\} - \{\mathbf{F}_N\} = \{\mathbf{F}\} \quad (26)$$

where  $[\bar{\mathbf{K}}_L] = \sum_e [\bar{\mathbf{K}}_L]_e =$  structure linear coefficient matrix;  $[\mathbf{K}_N] = \sum_e [\mathbf{K}_N]_e =$  structure nonlinear coefficient matrix;  $\{\mathbf{F}_N\} = \sum_e \{\mathbf{f}_N\}_e =$  nonlinear component of the thermal load vector;  $\{\mathbf{F}\} = \{\mathbf{F}^U\} + \{\mathbf{F}^\theta\}$ ;  $\{\mathbf{F}^U\} =$  nodal mechanical and electric load vector; and  $\{\mathbf{F}^\theta\} = \sum_e \{\mathbf{f}^\theta\}_e =$  linear component of thermal and pyroelectric load vector.

## 5. Buckling Analysis

At static equilibrium, i.e., when the internal and external forces are balanced, the system of nonlinear equations becomes

$$[\mathbf{K}_T]\{\Delta\mathbf{U}\} = \{\mathbf{0}\} \quad (27)$$

When the plate is subjected to inplane loads only, i.e., when the transverse displacements are zero, the nonlinear stiffness component in the tangent stiffness matrix does not exist. If the inplane stresses can lead to buckling, then an eigenproblem exists

$$[[\bar{\mathbf{K}}_L] + \lambda[\mathbf{K}_\sigma]]\{\Delta\mathbf{U}\} = \{\mathbf{0}\} \quad (28)$$

where  $\lambda$  is the inplane stress magnification factor. The objective of the eigenproblem is to calculate values of  $\lambda$  that make the tangent stiffness matrix singular thereby introducing instability in the plate. Thus, critical buckling loads and associated mode shapes correspond to the eigenvalues and eigenvectors of (28). Expanding equation (28) gives

$$\left( \begin{array}{cc} [\bar{K}^{uu}] & [\bar{K}^{u\psi}] \\ [\bar{K}^{u\psi}]^T & [\bar{K}^{\psi\psi}] \end{array} \right) - \lambda \begin{pmatrix} [K_{\sigma}^u] & [0] \\ [0] & [0] \end{pmatrix} \left\{ \begin{array}{c} \{\Delta u\} \\ \{\Delta \psi\} \end{array} \right\} = \{0\} \quad (29)$$

where  $[K_{\sigma}^u]$  is the assembled geometric stiffness matrix associated with the displacement

degrees of freedom, i.e.,  $[K_{\sigma}]_e = \int_a \begin{pmatrix} [G]^T [\hat{N}] [G] & [0] \\ [0] & [0] \end{pmatrix} da$  = element geometric stiffness

matrix;  $[G] = [[G_1] \ [G_2] \ \dots \ [G_{nen}]]$ ;  $[G]_i = \begin{bmatrix} 0 & 0 & \frac{\partial N_i}{\partial x} & 0 & 0 \\ 0 & 0 & \frac{\partial N_i}{\partial y} & 0 & 0 \end{bmatrix}$ ; and  $[\hat{N}] =$

$\begin{pmatrix} N_x & N_{xy} \\ N_{xy} & N_y \end{pmatrix}$  = inplane stress resultant matrix with  $N_{\alpha} = N_{\alpha}^u + N_{\alpha}^{\psi} - N_{\alpha}^{\theta}$ ,  $\alpha = x, y$  or  $xy$ .

Since buckling is an elasticity phenomenon, condensation of the electric potential degrees of freedom does not alter the eigenproblem. Condensation is at the global level.

Equation (29) after condensation becomes

$$\left[ [\bar{K}_L^u] - \lambda [K_{\sigma}^u] \right] \{\Delta u\} = \{0\} \quad (31)$$

where  $[\bar{K}_L^u] = [\bar{K}^{uu}] - [\bar{K}^{\psi u}]^T [\bar{K}^{\psi\psi}]^{-1} [\bar{K}^{\psi u}]$ .

The geometric stiffness matrix is a function of inplane stress resultants. A first step in the buckling analysis is the linear elastic analysis of the plate under the action of inplane loads to calculate the inplane stresses and subsequently the geometric stiffness matrix. In the

second step, calculation of the buckling loads and corresponding mode shapes follows from equation (31).

An alternate method for computing the critical load is nonlinear buckling analysis. This alternate procedure involves subjecting the plate to an inplane load and a small notional transverse load. Then perform an incremental/iterative nonlinear analysis, which is based on the explicit iteration on spheres algorithm of Forde and Stiemer (1987) and is described in detail in Blandford (1996) and Datchanamourty (2008). At the point where the stiffness matrix approaches a singularity, a small perturbation in the transverse load leads to an enormous increase in the transverse displacement. Such a behavior in the load-deflection curve signifies points of instability. The response after oscillating about unstable points slowly stabilizes into an equilibrium path with subsequent load steps and iterations.

## 6. Numerical Results

The mechanically loaded problem is a simply supported six-layer symmetric composite (PZT5/0/90)s subjected to uniaxial inplane line load (Varelis and Saravanos, 2002). The material properties of the Graphite/Epoxy layer are  $E_1 = 132.4$  GPa;  $E_2 = 10.8$  GPa;  $G_{12} = G_{13} = 5.6$  GPa;  $G_{23} = 3.6$  GPa; and  $\nu_{12} = 0.24$ . Material properties of the piezoelectric layer (PZT5) are  $E_1 = 62$  GPa;  $E_2 = 62$  GPa;  $G_{12} = G_{13} = 23.6$  GPa;  $G_{23} = 18$  GPa;  $\nu_{12} = 0.31$ ;  $d_{31} = d_{32} = -220 \times 10^{-12}$  m/V;  $d_{24} = d_{15} = 670 \times 10^{-12}$  m/V; and  $\eta_{11} = \eta_{22} = \eta_{33} = 2598 \eta_0$  where  $\eta_0 = 8.85 \times 10^{-12}$  F/m. Dimensions of the plate are  $a = b = 0.2$  m and  $h = 0.001$  m.

Table 1 shows the critical buckling load multipliers for the first four modes in the x-axis i.e., (1, 1), (2, 1), (3, 1) and (4, 1) based on a uniaxial compressive load of 1 kN/m.

Varelis and Saravanos (2002) compared their uncoupled results with analytical elasticity

solutions of Whitney (1987). The finite element solutions of Varelis and Saravanos uses an 8 x 8 mesh of eight-node two-dimensional serendipity elements while in the current research (Mixed Formulation) nine-node Lagrangian hierarchical elements are employed with the same mesh density. The first three buckling modes of the uncoupled analysis predicted by both formulations agree closely, less than one-half percent difference, with the analytical solution. For the fourth mode, the mixed formulation result is slightly more accurate (1.14% difference) than the solution of Varelis and Saravanos (-1.84% difference). The mixed formulation results show good agreement with the coupled solutions of Varelis and Saravanos (2002) as shown by comparing the two “C” columns in Table 1. Slight differences could be due to the slightly more accurate nine-node Lagrangian element versus the eight-node serendipity element used by Varelis and Saravanos. Table 1 also presents the critical buckling loads based on 8 x 8 mesh of cubic and quartic elements. Buckling loads for the first three modes show negligible difference compared to the analytical results. A difference of less than -0.25% is observed for the fourth mode in the case of cubic and quartic hierarchic elements.

An 8 x 8 mesh of nine-node Lagrangian elements is used on the full plate for the nonlinear buckling analysis with coupled and uncoupled effects. As given by the eigenvalue analysis, the nonlinear response predicts the various buckling modes. The effect of piezoelectric coupling as shown in Figure 4 is to increase the buckling load. For the problem under consideration, a change of 35% is observed in the buckling load due to the piezoelectric coupling.

To investigate the piezoelectric coupling effect for self-strain buckling problems (thermal and piezoelectric), an eight-layer symmetric laminate (0/90/0/90)<sub>s</sub>, with

piezoelectric layers at the top and bottom thus making it a ten-layer composite, is considered.

Material properties of the lamina are  $E_1 = 138$  GPa;  $E_2 = 8.28$  GPa;  $G_{12} = G_{13} = G_{23} = 6.90$

GPa;  $\nu_{12} = 0.33$ ;  $\alpha_1 = 0.18 \times 10^{-6} / ^\circ\text{C}$ ; and  $\alpha_2 = 27.0 \times 10^{-6} / ^\circ\text{C}$ . Piezoelectric material

properties for the isotropic PVDF material are  $E_1 = E_2 = E_3 = 2$  GPa;  $\nu_{12} = \nu_{13} = \nu_{23} = 0.333$ ;

$G_{12} = G_{13} = G_{23} = 0.75$  GPa;  $\alpha_1 = \alpha_2 = \alpha_3 = 1.2 \times 10^{-4} / ^\circ\text{C}$ ;  $d_{31} = d_{32} = 23 \times 10^{-12} \text{ } ^\circ\text{C}/\text{N}$ ;  $d_{24} =$

$d_{15} = -23 \times 10^{-12} \text{ } ^\circ\text{C}/\text{N}$ ;  $\eta_{11} = \eta_{22} = \eta_{33} = 1 \times 10^{-10} \text{ F}/\text{m}$ ; and  $p_3 = -2.5 \times 10^{-5} \text{ } ^\circ\text{C}/\text{K}/\text{m}^2$ .

Piezoelectric material properties for the isotropic PZT are  $E_1 = E_2 = E_3 = 60$  GPa;  $\nu_{12} = \nu_{13} =$

$\nu_{23} = 0.333$ ;  $G_{12} = G_{13} = G_{23} = 22.5$  GPa;  $\alpha_1 = \alpha_2 = \alpha_3 = 1.2 \times 10^{-6} / ^\circ\text{C}$ ;  $\eta_{11} = \eta_{22} = \eta_{33} = 1.5$

$\times 10^{-8} \text{ F}/\text{m}$ ;  $d_{31} = d_{32} = -1.75 \times 10^{-10} \text{ } ^\circ\text{C}/\text{N}$ ,  $d_{24} = d_{15} = 6.0 \times 10^{-10} \text{ } ^\circ\text{C}/\text{N}$ , and  $p_3 = 7.5 \times 10^{-4}$

$^\circ\text{C}/\text{K}/\text{m}^2$ .

Validation of the uncoupled results uses the analytical results of Jonnalagadda (1993).

Additionally, piezoelectric coupling effects are investigated. Table 2 shows the thermal

buckling results using a 4 x 4 mesh of quadratic elements for various a/h ratios of the

symmetric composite with PVDF layers on top and bottom. Critical thermal buckling loads

are nondimensionalized as

$$\bar{T} = \theta \alpha_0 \left( \frac{a}{h} \right)^2 \quad (14)$$

where  $\alpha_0 = 1.2 \times 10^{-4} / ^\circ\text{C}$ . Table 2 shows excellent agreement (errors  $\ll 1\%$ ) between the

finite element and first-order shear deformation theory analytical solutions. For the PVDF

laminate, the piezoelectric coupling effect increases the buckling load by approximately 3%.

Table 3 shows the thermal buckling load for the same laminate configuration but with

PZT layers on top and bottom. It is interesting to note that piezoelectric coupling reverses

the inplane stresses induced in the PZT layers, which leads to negative buckling loads for the

various  $a/h$  ratios. This is due to the pyroelectric coefficient of the PZT material being positive as opposed to negative for PVDF materials. Ignoring the sign change, the coupled buckling results are 64.6% to 68.9% higher than the corresponding uncoupled buckling loads for  $10 \leq a/h \leq 1000$  ( $(\text{coupled result} - \text{uncoupled result})/\text{uncoupled result}$ ).

Nonlinear thermal buckling analysis is performed by applying a uniform temperature on the top and bottom surfaces of piezothermoelastic laminates in addition to a small notional transverse mechanical load. All the critical loads considered for the PVDF laminate matched the buckling results. Figure 5 shows the nonlinear calculated results for  $a/h$  ratio of 40. This result, and others not included, show that the nonlinear analysis predicts the same buckling load as does the eigenvalue problem for the thermally loaded PVDF laminated for both uncoupled and coupled analyses.

Table 4 records piezoelectric buckling results for the eight-layer symmetric laminate with PVDF piezoelectric layers at the top and bottom of the laminate subjected to opposite electric potentials on the top and bottom surfaces of the laminate. Nondimensionalized critical electric potentials are

$$\bar{\psi} = \psi d_0 \left( \frac{a}{h} \right)^3 \quad (15)$$

where  $d_0 = 10^{-11} \text{ } ^\circ\text{C}/\text{N}$ . A  $4 \times 4$  quadratic element mesh is used in the finite element analysis and the results are in excellent agreement with theoretical results. Table 4 shows that the nondimensionalized buckling load changes little for  $a/h \geq 60$ .

## 7. Summary and Conclusions

This paper has focused on using a hierarchic finite element formulation for the geometric nonlinear analysis of piezothermoelastic composite plates subjected to both

mechanical and self-strain (thermal and electric field) loadings for the determination of the buckling loads for smart composite plate structures. Geometric nonlinearity has been included in the von Karman sense, i.e., large transverse displacements with small inplane displacements. A mixed formulation in which an independent discretization of the transverse shear stress resultants at the Gauss integration points using standard Lagrangian interpolation in addition to the displacement, rotation, and electric potential variables expressed in terms of hierarchic finite elements (quadratic, cubic and quartic) have been used to construct the element level algebraic equations. Thermoelastic and pyroelectric effects are part of the constitutive equations. Since the buckling load multiplier does not multiply the electric potential variables, condensation of these variables is at the global level.

Results for mechanically and self-strained (thermal and electric field) loaded composite plates have been presented. The results demonstrate the impact of piezoelectric coupling on the buckling load magnitudes by calculating the buckling loads that include the piezoelectric effect (coupled) and exclude the effects (uncoupled).

As would be expected, the relatively weak PVDF layers do not significantly alter the calculated results when considering piezoelectric coupling. The net increase is about 3% for the thermal loaded ten-layer laminate (PVDF/0/90/0/90)<sub>s</sub>.

However, adding the relatively stiff PZT as the top and bottom layers produces significant differences between the uncoupled and coupled results. For the mechanically loaded six-layer laminate (PZT/0/90)<sub>s</sub> (Varelis and Saravanos, 2002) results in a buckling load increase of over 30% for the first four buckling modes of the uniaxially compressed plate. For the thermally loaded ten-layer laminate (PZT/0/90/0/90)<sub>s</sub>, a reversal of stress is required to cause buckling in the coupled analyses due to the sign on the pyroelectric

constant for the PZT material. Neglecting the sign change, an increase of approximately 67% is observed in the absolute buckling load magnitude for the coupled analysis compared with the uncoupled analysis.

Determining the buckling loads via geometric nonlinear analysis with small, mechanical notational loads has been shown to produce essentially the same answers as predicted by eigenvalue analysis for composite laminates with either PVDF or PZT piezoelectric materials on the top and bottom surfaces.

## **Acknowledgements**

The authors wish to acknowledge the financial support provided by the University of Kentucky Center for Computational Sciences for partial support of the research reported in this paper. The views contained herein are those of the authors and should not be interpreted as necessarily representing the official policies or endorsements, either expressed or implied, of the University of Kentucky, Center for Computational Sciences.

## **REFERENCES**

Blandford, GE, Progressive Failure Analysis of Inelastic Space Truss Structures. *Computers and Structures*, 1996; 58(5): 981-980.

Chandrashekhara K, Buckling of Multi-Layered Composite Plates Under Uniform Temperature Field. In: Birman V, Hui D, editors, *Thermal Effects on Structures and Materials*. ASME PVP 203, AMD 110, 1990; 29-33.

Chen LW, Chen LY, Thermal Buckling Analysis of Composite Laminated Plates by the Finite Element Method. *Journal of Thermal Stresses*, 1989; 12: 41-56.

Chen WJ, Lin PD, Chen LW, Thermal Buckling Behavior of Thick Laminated Plates Under Nonuniform Temperature Distribution. *Computers and Structures*, 1991; 41(4): 637-645.

Datchanamourty B, Nonlinear Static, Buckling and Dynamic Analysis of Laminated Piezothermoelastic Composite Plate Using Reissner-Mindlin Theory Based on a Mixed Hierarchic Finite Element Formulation, Ph.D., Civil Engineering, May 2008.

Dawe DJ, Ge YS, Thermal Buckling of Shear-Deformable Composite Laminated Plates by the Spline Finite Strip Method. *Computer Methods in Applied Mechanics and Engineering*, 2000; 185: 347-366.

Forde BWR, Stiemer SF, Improved Arc Length Orthogonality Methods for Nonlinear Finite Element Analysis. *Computers and Structures* 1987; 27: 625-630.

Gossard ML, Seide P, Roberts WM, Thermal Buckling of Plates. NACA TN, 2771, 1952.

Huang NN, Tauchert TR, Thermal Buckling of Clamped Symmetric Laminated Plates. *Thin-Walled Structures*, 1992; 13(4): 259-273.

Jonnalagadda KD, Development of Higher-Order Plate Theories and Applications to Piezothermoelastic Laminates. Master of Science Thesis, University of Kentucky, Lexington, KY, 1993.

Jonnalagadda, KD, Blandford, GE, Tauchert, TR, Piezothermoelastic Composite Plate Analysis Using First-Order Shear Deformation Theory. *Computers and Structures*, 1994; 51(1): 79-89.

Kabir HRH, Hamad MAM, Al-Duaij J, John MJ, Thermal Buckling Response of All-Edge Clamped Rectangular Plates with Symmetric Angle-Ply Lamination. *Composite Structures*, 2007; 79(1): 148-155.

Reddy JN, *Mechanics of Laminated Composite Plates: Theory and Analysis*. New York: CRC Press, Second Edition, 2004.

Noor AK, Peters JM, Thermomechanical Buckling of Multilayered Composite Plates. *Journal of Engineering Mechanics*, ASCE, 1992; 118: 351-366.

Prabhu MR, Dhanaraj R, Thermal Buckling of Laminated Composite Plates. *Computers and Structures*, 1994; 53(5): 1193-1204.

Shukla KK, Nath Y, Buckling of Laminated Composite Rectangular Plates Under Transient Thermal Loading. *Journal of Applied Mechanics*, 2002; 69(5): 684-692.

Tauchert TR, Thermal Buckling of Thick Antisymmetric Angle-Ply Laminates. *Journal of Thermal Stresses*, 1987; 10: 113-124.

Tauchert TR, Huang NN. Thermal Buckling of Symmetric Angle-Ply Laminated Plates. In: Marshal IN, editor. *Composite Structures, Proceedings of the Fourth International Conference on Composite Structures*, Paisley, U.K.: Elsevier, 1987; 1424–1435.

Thangaratnam KR, Palaninathan R, Ramachandran J, Thermal Buckling of Composite Laminated Plates. *Computers and Structures*, 1989; 32(5): 1117-1124.

Timoshenko SP, Gere JM, *Theory of Elastic Stability*. Second Edition, New York: McGraw-Hill, Second Edition, 1961.

Tzou HS, Zhou YH, Nonlinear Piezothermoelasticity and Multi-Field Actuations, Part 2: Control of Nonlinear Buckling and Dynamics. *ASME Transaction, Journal of Vibration and Acoustics*, 1997; 119: 382-389.

Varelis D, Saravanos DA, Nonlinear Coupled Mechanics and Initial Buckling of Composite Plates with Piezoelectric Actuators and Sensors. *Journal of Smart Materials and Structures* 2002; 11: 330-336.

Varelis D, Saravanos DA, Coupled Buckling and Post-Buckling Analysis of Active Laminated Piezoelectric Composite Plates. *International Journal of Solids and Structures*, 2004; 41: 1519-1538.

Whitney JM, *Structural Analysis of Laminated Anisotropic Plates*. Lancaster, PA; Technomic: 1987.

Zeinkiewicz OC, Taylor RL, *The Finite Element Method, Volume 1 The Basis*. Boston: Butterworth-Heinemann, Fifth Edition, 2000.

# Figure Captions

Figure 1. Layout of an N-layer Composite Laminate

Figure 2. Hierarchic Lagrangian Finite Elements

Figure 3. Transverse Shear Stress Resultant Interpolation Points

Figure 4. Nonlinear Buckling Response for a Symmetric Piezoelectric Composite Laminate (PZT/0/90)s Subjected to a Uniaxial Line Load ( $Q_{\text{ref}} = -1 \text{ kN/m}$ )

Figure 5. Nonlinear Thermal Buckling for a Ten-Layer Symmetric Piezoelectric Composite Laminate (PVDF/0/90/0/90)s for  $a/h = 40$

Table 1. Critical Buckling Loads (kN/m) of a Symmetric Piezoelectric Composite Laminate (PZT/0/90)s Subjected to a Uniaxial Line Load

Mode	Analytical	Varelis and Saravanos (2002) (Quadratic)		Mixed Formulation (Quadratic)		Mixed Formulation (Cubic)		Mixed Formulation (Quartic)	
	UC <sup>1</sup>	UC <sup>1</sup>	C <sup>2</sup>	UC <sup>1</sup>	C <sup>2</sup>	UC <sup>1</sup>	C <sup>2</sup>	UC <sup>1</sup>	C <sup>2</sup>
(1,1)	5.37	5.33	7.22	5.37	7.27	5.37	7.27	5.37	7.27
(2,1)	9.00	8.98	11.94	9.01	11.97	9.00	11.96	9.00	11.96
(3,1)	16.50	16.50	21.80	16.56	21.82	16.49	21.74	16.49	21.74
(4,1)	27.20	26.70	35.60	27.51	36.11	27.15	35.66	27.14	35.65

<sup>1</sup>UC ≡ Uncoupled Piezoelectric Analysis

<sup>2</sup>C ≡ Coupled Piezoelectric Analysis

Table 2. Nondimensionalized Thermal Buckling Loads ( $\bar{T}$ ) for a Ten-Layer Symmetric Piezoelectric Composite Laminate (PVDF/0/90/0/90)s

a/h	Analytical	MF <sup>1</sup>	
	UC <sup>2</sup>	UC <sup>2</sup>	C <sup>3</sup>
5	1.457	1.457	1.502
10	1.811	1.813	1.869
15	1.898	1.899	1.958
20	1.930	1.932	1.992
25	1.946	1.947	2.008
30	1.954	1.956	2.016
35	1.960	1.961	2.022
40	1.963	1.964	2.025
60	1.969	1.970	2.031
80	1.971	1.972	2.034
100	1.972	1.973	2.035
1000	1.973	1.975	2.037

<sup>1</sup>MF  $\equiv$  Mixed Formulation

<sup>2</sup>UC  $\equiv$  Uncoupled Piezoelectric Analysis

<sup>3</sup>C  $\equiv$  Coupled Piezoelectric Analysis

Table 3. Nondimensionalized Thermal Buckling Loads ( $\bar{T}$ ) for a Ten-Layer Symmetric Piezoelectric Composite Laminate (PZT/0/90/0/90)s

a/h	MF <sup>1</sup>	
	UC <sup>2</sup>	C <sup>3</sup>
5	4.208	-6.584
10	5.475	-9.010
15	5.799	-9.675
20	5.922	-9.931
25	5.981	-10.055
30	6.013	-10.123
35	6.033	-10.165
40	6.045	-10.192
60	6.069	-10.242
80	6.077	-10.260
100	6.081	-10.268
1000	6.088	-10.283

<sup>1</sup>MF  $\equiv$  Mixed Formulation

<sup>2</sup>UC  $\equiv$  Uncoupled Piezoelectric Analysis

<sup>3</sup>C  $\equiv$  Coupled Piezoelectric Analysis

Table 4. Nondimensionalized Electric Potentials ( $\bar{\psi}$ ) of a Ten-Layer Symmetric Piezoelectric Composite Laminate (PVDF/0/90/0/90)s Under Piezoelectric Buckling

a/h	Analytical	MF <sup>1</sup>
5	2.138	2.139
10	2.659	2.661
15	2.786	2.788
20	2.834	2.836
25	2.856	2.858
30	2.868	2.871
35	2.876	2.878
40	2.881	2.883
60	2.890	2.892
80	2.893	2.895
100	2.894	2.897
1000	2.897	2.899

<sup>1</sup>MF  $\equiv$  Mixed Formulation

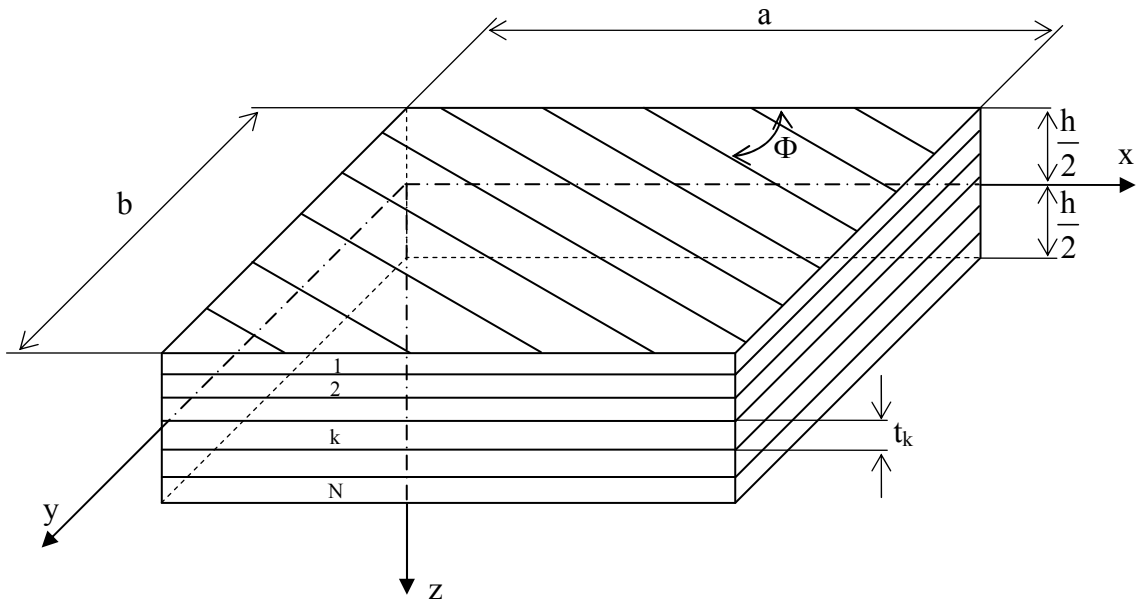
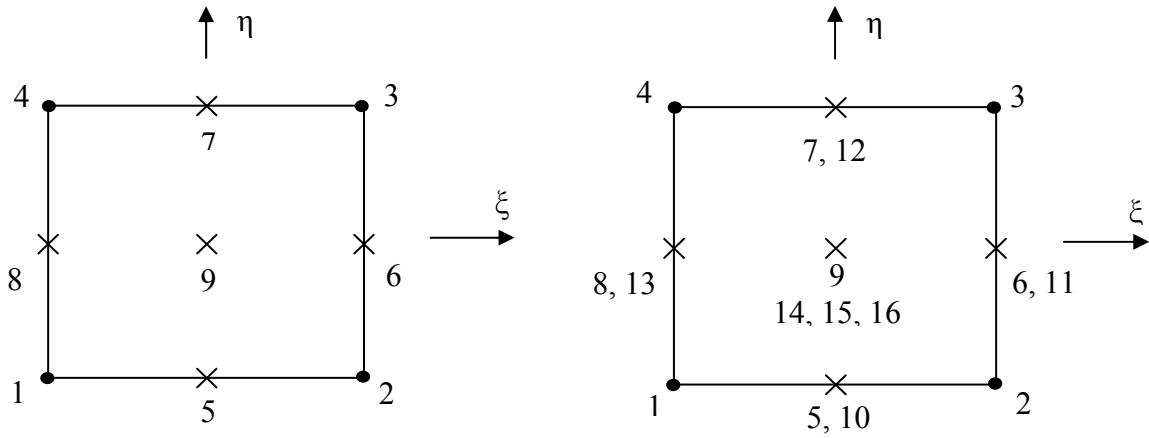
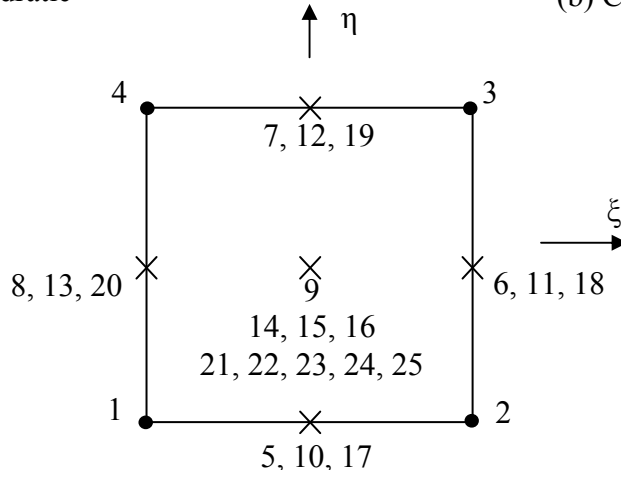


Figure 1. Layout of an N-layer Composite Laminate



(a) Quadratic

(b) Cubic



(c) Quartic

- Corner Node
- × Hierarchic Node

a. Hierarchic Lagrangian Element Nodes

$$N_1 = \frac{1}{4}(1-\xi)(1-\eta) \quad N_2 = \frac{1}{4}(1+\xi)(1-\eta)$$

$$N_3 = \frac{1}{4}(1+\xi)(1+\eta) \quad N_4 = \frac{1}{4}(1-\xi)(1+\eta)$$

Corner node shape functions

$$N_5 = \frac{1}{4}(\xi^2-1)(1-\eta) \quad N_6 = \frac{1}{4}(1+\xi)(\eta^2-1)$$

$$N_7 = \frac{1}{4}(\xi^2-1)(1+\eta) \quad N_8 = \frac{1}{4}(1-\xi)(\eta^2-1)$$

$$N_9 = \frac{1}{4}(\xi^2-1)(\eta^2-1)$$

Quadratic hierarchic shape functions

$$N_{10} = \frac{1}{12}(\xi^3-\xi)(1-\eta) \quad N_{11} = \frac{1}{12}(1+\xi)(\eta^3-\eta)$$

$$N_{12} = \frac{1}{12}(\xi^3-\xi)(1+\eta) \quad N_{13} = \frac{1}{12}(1-\xi)(\eta^3-\eta)$$

$$N_{14} = \frac{1}{12}(\xi^3-\xi)(\eta^2-1) \quad N_{15} = \frac{1}{12}(\xi^2-1)(\eta^3-\eta)$$

$$N_{16} = \frac{1}{36}(\xi^3-\xi)(\eta^3-\eta)$$

Cubic hierarchic shape functions

$$N_{17} = \frac{1}{48}(\xi^4-1)(1-\eta) \quad N_{18} = \frac{1}{48}(\eta^4-1)(1+\xi)$$

$$N_{19} = \frac{1}{48}(\xi^4-1)(1+\eta) \quad N_{20} = \frac{1}{48}(\eta^4-1)(1-\xi)$$

$$N_{21} = \frac{1}{48}(\xi^4-1)(\eta^2-1) \quad N_{22} = \frac{1}{48}(\eta^4-1)(\xi^2-1)$$

$$N_{23} = \frac{1}{144}(\xi^4-1)(\eta^3-\eta) \quad N_{24} = \frac{1}{144}(\eta^4-1)(\xi^3-\xi)$$

$$N_{25} = \frac{1}{576}(\xi^4-1)(\eta^4-1)$$

Quartic hierarchic shape functions

b. Hierarchic Lagrangian Shape Functions

Figure 2. Hierarchic Lagrangian Finite Elements

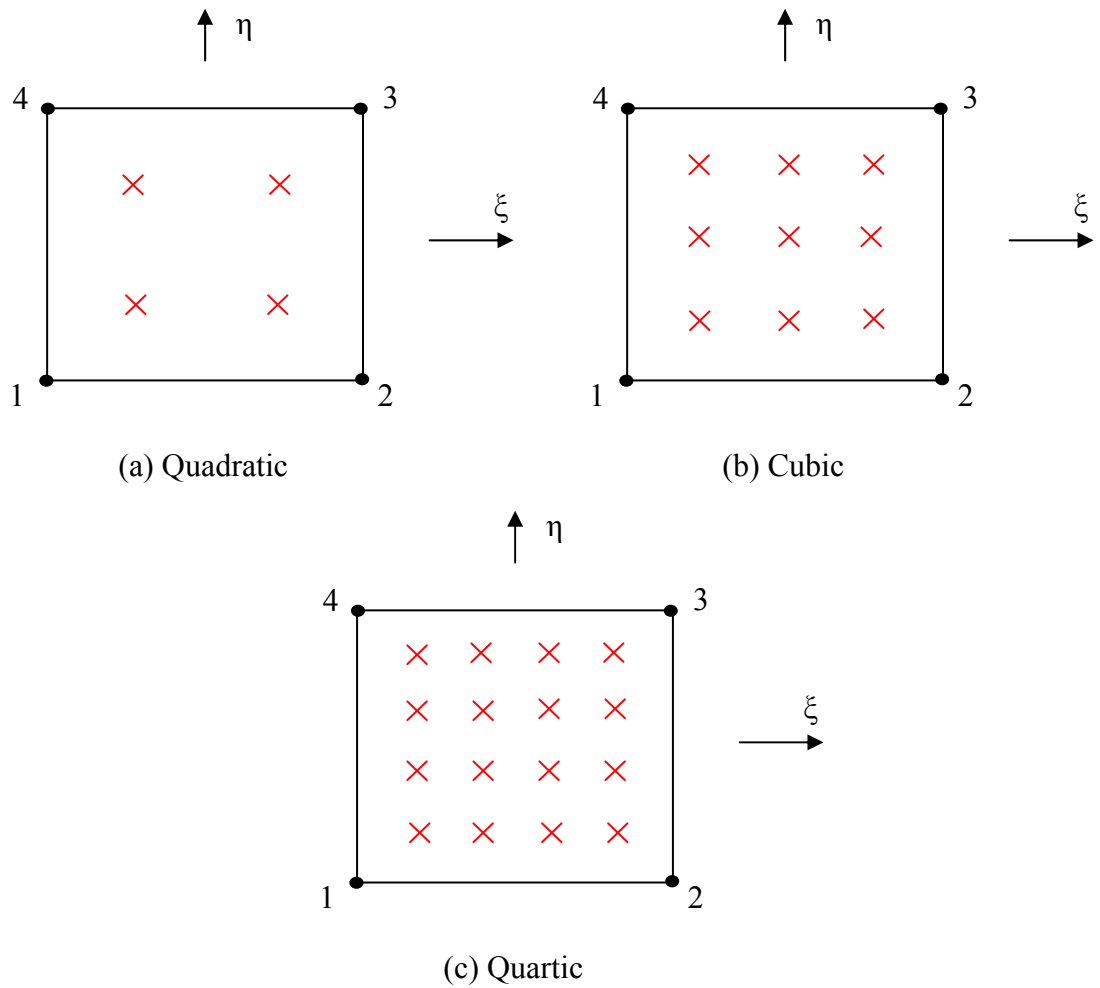


Figure 3. Transverse Shear Stress Resultant Interpolation Points

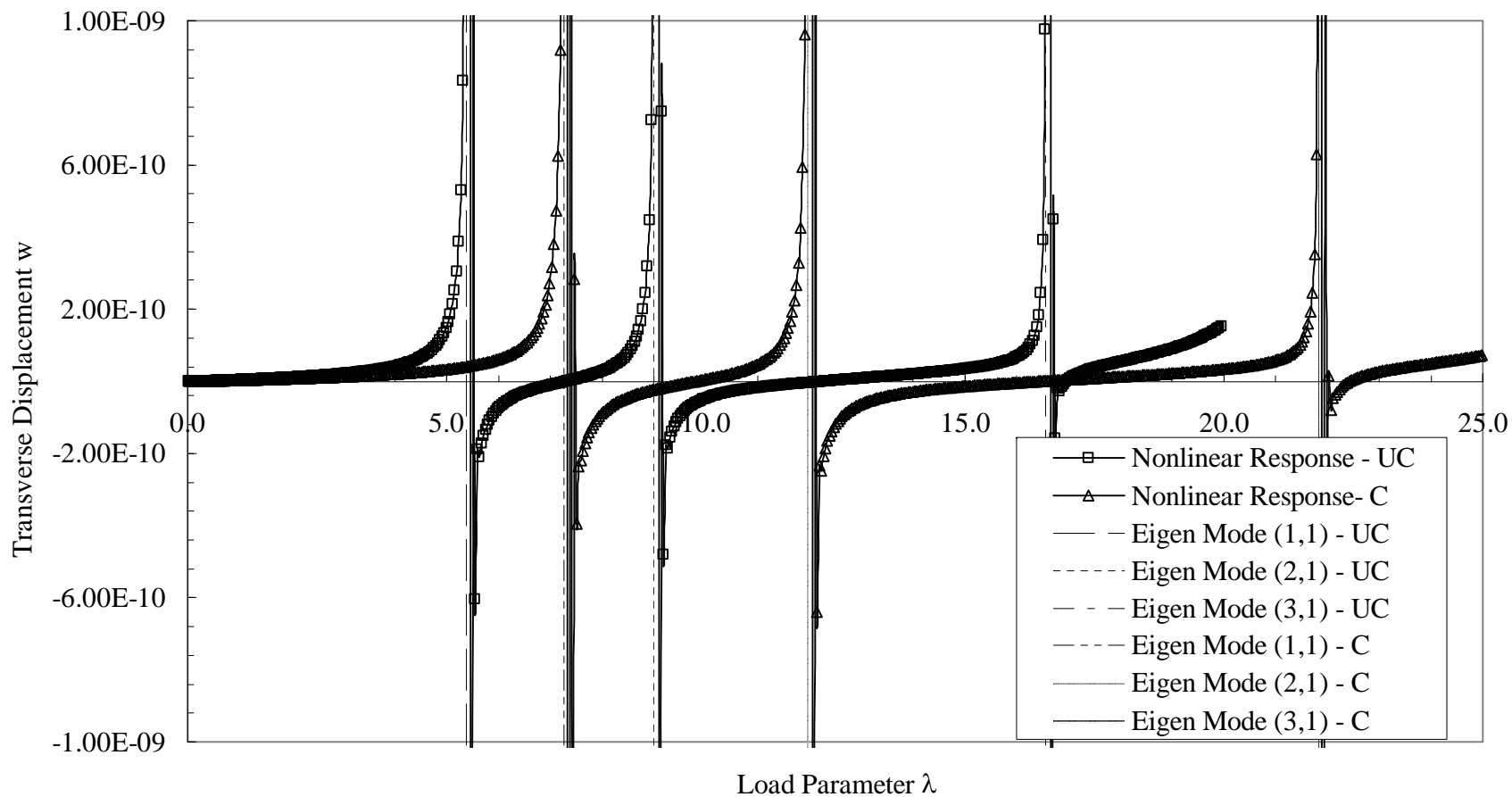


Figure 4. Nonlinear Buckling Response for a Symmetric Piezoelectric Composite Laminate (PZT/0/90)<sub>s</sub> Subjected to a Uniaxial Line Load ( $Q_{ref} = -1$  kN/m)

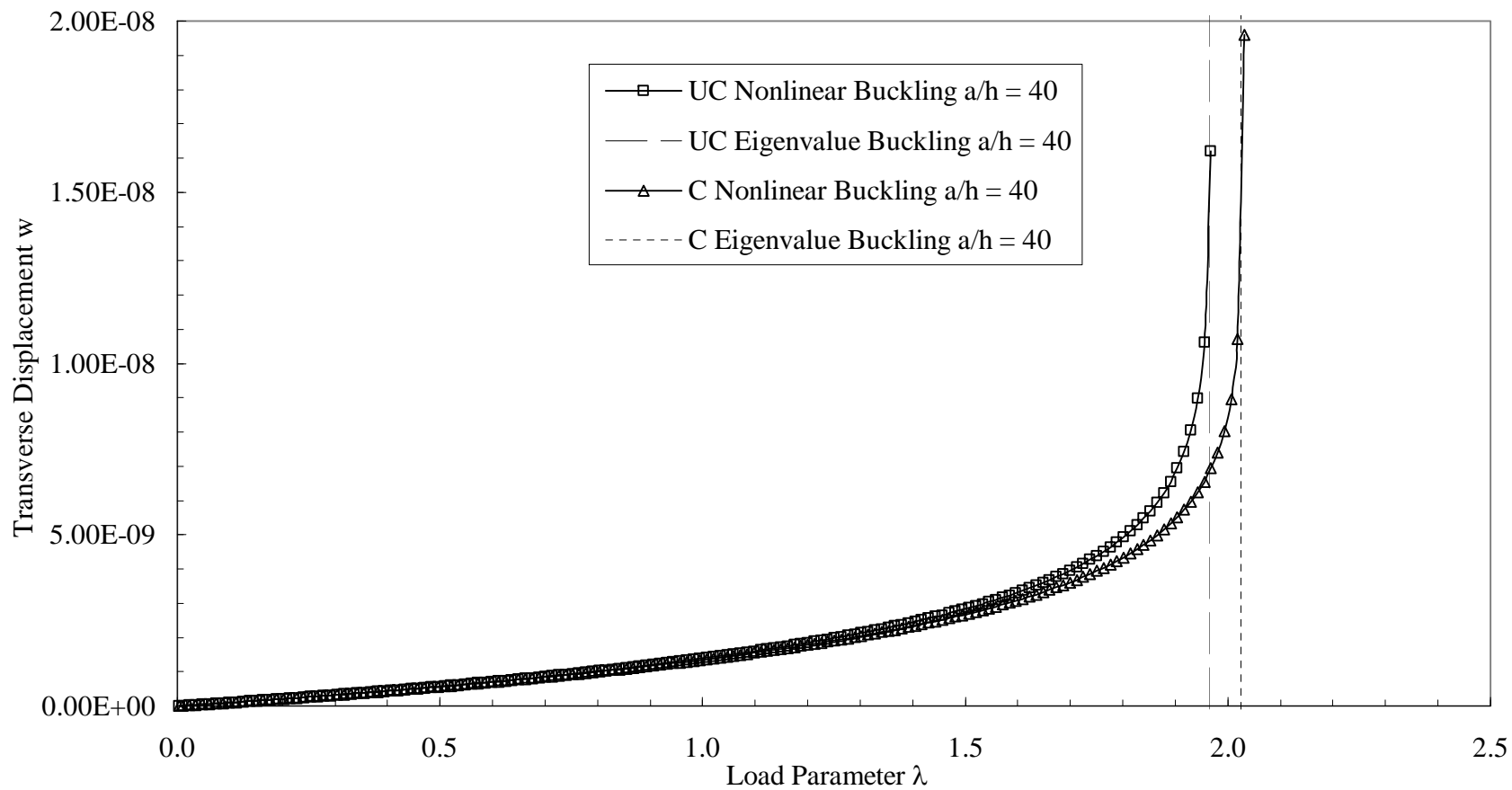


Figure 5. Nonlinear Thermal Buckling for a Ten-Layer Symmetric Piezoelectric Composite Laminate (PVDF/0/90/0/90)<sub>s</sub> for  $a/h = 40$